LBL-29877
UC-404

Lawrence Berkeley Laboratory
UNIVERSITY OF CALIFORNIA

Materials Sciences Division
National Center for Electron Microscopy

Published in Nature, Vol. 348, No. 6301, p. 525 (1990)

Resolution of Oxygen Atoms in Staurolite by Three-Dimensional Transmission Electron Microscopy

K.H. Downing, H. Meisheng, H.-R. Weng, M.A. O'Keefe

October 1990

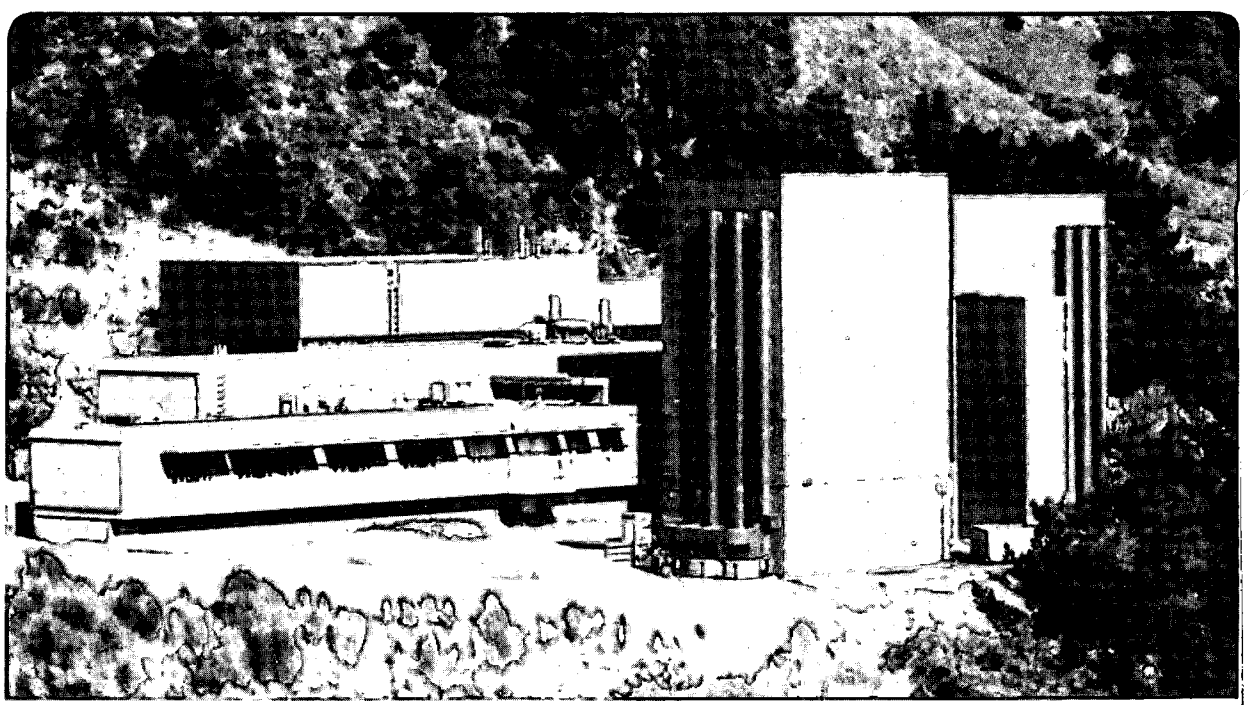

LOAN COPY
Circulates
for 4 weeks
Bldg. 50 Library.
LBL-29877
Copy 2

Prepared for the U.S. Department of Energy under Contract Number DE-AC03-76SF00098

DISCLAIMER

This document was prepared as an account of work sponsored by the United States Government. While this document is believed to contain correct information, neither the United States Government nor any agency thereof, nor the Regents of the University of California, nor any of their employees, makes any warranty, express or implied, or assumes any legal responsibility for the accuracy, completeness, or usefulness of any information, apparatus, product, or process disclosed, or represents that its use would not infringe privately owned rights. Reference herein to any specific commercial product, process, or service by its trade name, trademark, manufacturer, or otherwise, does not necessarily constitute or imply its endorsement, recommendation, or favoring by the United States Government or any agency thereof, or the Regents of the University of California. The views and opinions of authors expressed herein do not necessarily state or reflect those of the United States Government or any agency thereof or the Regents of the University of California.

LBL-29877

Resolution of Oxygen Atoms in Staurolite by Three-Dimensional Transmission Electron Microscopy

K.H. Downing*, H. Meisheng+, H.-R. Weng+ and M.A. O'Keefe

Materials Science Division
National Center for Electron Microscopy
Lawrence Berkeley Laboratory
University of California, Berkeley, CA 94720

*Donner Laboratory
Lawrence Berkeley Laboratory
University of Californi
Berkeley, CA 94720

+University of California
Dept. of Geology & Geophysics
Berkeley, CA 94720

Nature, Vol. **348**, No. 6301, p.525 (1990)

This work was supported in part by National Science Foundation, Grant EAR 88-16577, National Institutes of Health Grant GM-36884, and the Director, Office of Energy Research, Office of Basic Energy Sciences, Materials Science Division of the U.S. Department of Energy under Contract No. DE-AC03-76SF00098.

Resolution of oxygen atoms in staurolite by three-dimensional transmission electron microscopy

Kenneth H. Downing
Donner Laboratory, Lawrence Berkeley Laboratory, Berkeley, CA 94720

Hu Meisheng and Hans-Rudolf Wenk
Department of Geology and Geophysics, University of California, Berkeley, CA 94720

Michael A. O'Keefe
National Center for Electron Microscopy, Lawrence Berkeley Laboratory, Berkeley, CA 94720

Abstract. A three dimensional reconstruction of the crystal structure of staurolite, including oxygen atom positions, was obtained from high resolution transmission electron micrographs, providing both phases and amplitudes of the structure factors. The method opens the possibility of performing crystal structure determinations on volumes too small for X-ray methods.

Submitted to *Nature*

With advances in electron microscope design, high resolution electron microscopy has become routine, and point resolutions of less than 2Å have been obtained in many inorganic crystals[1-4]. The images provide a representation of the Coulomb potential (essentially the electron density), but interpretation generally requires comparison of experimental images with calculations[5]. Since the images are two-dimensional representations of the full three-dimensional structure, information is invariably lost. In particular, oxygen atoms are normally not seen. The technique of electron crystallography, in which information from several views of a crystal is combined, has been developed to obtain three-dimensional information on proteins[6-8]. Here we use this technique to obtain a three-dimensional reconstruction of the crystal structure of staurolite, a silicate mineral. We are able to identify the positions of oxygen atoms in the lattice. These results show the potential of the method for high-resolution structure determination on samples that are too small for the use of X-ray techniques.

Electron crystallography is in many ways analogous to X-ray crystal structure determination, except that structure factor phases are determined directly from high resolution images. Because proteins are very susceptible to beam damage, most applications have provided resolution in the 10 - 20Å range which allows morphological domains to be distinguished. The first atomic model of a protein to be determined by electron crystallography was recently obtained for the membrane protein bacteriorhodopsin[9]. From the electron density map at 3.5Å resolution it was possible to trace the path of the polypeptide chain and define the location of amino acid side chains, although individual atoms could not be resolved. This same method should be applicable to other systems that are more stable in the electron beam and for which higher resolution can be obtained, provided that the effects of dynamical scattering can be minimized[10].

We have used this method to carry out a determination of the three-dimensional structure of staurolite to a resolution of 1.6Å. Staurolite, a silicate mineral for which the complex structure is well known[11], is typical of many oxide structures with close-packed oxygens surrounding different types of cations in tetrahedral and octahedral coordination.

Crystals of staurolite $HFe_2Al_9Si_4O_{24}$ from Alpe Sponda, Switzer-land, were sectioned perpendicular to the three main directions [100], [010], and [001], and electron transparent foils were prepared by ion beam thinning. The probable space group is $C2/m$, but deviations from the corresponding orthorhombic space group $Ccmm$ (a = 7.87, b = 16.62, c =

5.66Å) are minimal[11]. We have used orthorhombic symmetry in our calculations and representations. Using the JEOL ARM-1000 at the National Center for Electron Microscopy, we obtained focus series of images at atomic resolution in all three main directions. We also used the high angle tilt stage (± 40° on two axes) to obtain images perpendicular to [101] and [310]. We selected only micrographs in very thin areas (< 40Å) close to Scherzer focus for analysis.

An example is shown in Fig. 1a. In these thin areas, the scattering contribution from the amorphous film is considerable, but the crystalline component is resolved with a good signal-to-noise ratio. Images in each of the five projections were digitized and Fourier transformed, and the periodic structure reconstructed by inverse Fourier transformation of structure factors determined at the reciprocal lattice points[6] (Fig. 1b). Multibeam dynamical scattering image-contrast calculations[12] for the microscope conditions[13] and specimen parameters[11] agree well with the observed image (Fig. 1c). The same is true for diffraction patterns.

Figure 2a, 2b compares the experimental electron diffraction pattern with the calculated pattern. Also shown are a diffractogram obtained by optical diffraction from an experimental image and a diffractogram calculated for a 30Å-thick specimen (Fig. 2c,d). The optical diffractogram shows intensity to 1.4Å, which is the value at which the envelope of the contrast transfer function of the instrument approaches zero[13]. We used only reflections with $d > 1.6$Å in the present analysis because of the uncertainty in determining the sign of the CTF at high resolution. Symmetry-related reflections within each projection were averaged, then equivalent reflections in different projections were averaged, resulting in measurements of 30 of the 80 unique, non-extinct reflections out to $d = 1.6$Å.

Projections in five directions were combined to obtain data within the three-dimensional reciprocal space. For the reconstruction of the crystal electron potential $V(\boldsymbol{x})$ we apply the equation

$$V(\boldsymbol{x}) = \sum_{\mathbf{g}} |F_{\mathbf{g}}| e^{i\phi_{\mathbf{g}}} \cdot e^{-i2\pi \mathbf{g}\cdot\mathbf{x}}$$

where $|F_{\mathbf{g}}|$ is the amplitude of the structure factor, $\phi_{\mathbf{g}}$ the phase, and the summation is over all reciprocal lattice vectors, $\mathbf{g}$. Because all five of the projections of staurolite that we used are centrosymmetric, phases are either 0° or 180°. They are determined directly from the Fourier transform of the image after shifting to the proper phase origin[6]. Amplitudes $|F_{\mathbf{g}}|$ can be obtained either directly from the electron diffraction pattern (Fig. 2a) or from the transform of the image (Fig. 2c). We have used the latter. As electron diffraction patterns average over large areas of varying thickness, it is advantageous to obtain amplitude

information from images, even though they are affected by the contrast transfer function. The effect of this function on amplitudes could be corrected in the image transform, but we have not done so here because the main structural features rely much more on phases than on amplitudes. Calculations for staurolite show that amplitudes vary linearly with thickness up to 50Å; above that, changes are irregular due to dynamic scattering.

In the centrosymmetric case, phases derived from the images are less affected by dynamical effects. Table 1 compares, for some strong reflections of staurolite, computed amplitudes and phases with observed amplitudes and phases. Measured phases deviate from 0° or 180° as a result of the finite signal-to-noise ratio as well as slight misalignment of the electron beam and bending of the sample which cause deviations from centrosymmetry in the image. All of the measured phases, except for a few weak reflections, were within 30° of 0° or 180°, and when the centrosymmetry constraint was imposed, agreed with phases calculated from the known structure. Deviations between measured and observed amplitudes are larger, but as amplitudes mainly determine fine details in refinements, the effects of these deviations are too small to cause concern at this stage.

Symmetry operators expanded 30 structure factors to 72 in half space. With those we calculated a three-dimensional potential map. This is illustrated in Fig. 3 as a three-dimensional surface enclosing all of the cations and associated oxygens that are present at full occupancy. Because all atoms are located near z = 0 and z = 0.25, and because of the assumed orthorhombic symmetry, most of the information is contained in these two *xy* sections. Fig. 4a-d compares sections through the potential map with sections through the structure model. There is excellent correspondence between the experimental potential map and the crystal structure, with all atoms clearly resolved. The partially occupied octahedral Al site at $\frac{1}{2}$ $\frac{1}{2}$ 0 has a much lower potential than the fully occupied sites (e.g., $\frac{1}{2}$ $\frac{1}{6}$ 0). What surprises us most is the high resolution of light atoms such as oxygen, which can be clearly distinguished. The fact that individual atoms in a close-packed structure can be separated is largely attributed to the three-dimensional reconstruction. We see great potential for three-dimensional electron crystallography in determination of unknown crystal structures, particularly where homogeneous regions exist only in submicrometre-sized domains. Such heterogeneous crystals have been increasingly recognized in metals, ceramics and minerals. We estimate that a three-dimensional structure determination should be possible on areas only about 10 unit cells wide, provided that a sufficient number of projections can be recorded.

Acknowledgments: HRW remembers a PhD qualifying examination in Biophysics and discussions with Professor R. M. Glaeser which initiated this interdisciplinary research. KHD is supported in part by NIH grant GM 36884. Support from the National Science Foundation (EAR88 16577 to HRW), the University of California Education Abroad Program (to HM and HRW) is gratefully acknowledged. KHD, the NCEM and MAO'K are supported by the Director, Office of Energy Research, Office of Basic Energy Sciences, Materials Science Division, U.S. Dept. of Energy under Contract No. DE AC-03-76SF0098.

REFERENCES

1. Hashimoto, H., Endoh, H., Tanji, T., Ono, A., and Watanabe, E. *J. Phys. Soc. Japan* **42**, 1073-1074 (1977).

2. Smith, D. J., Camps, R. A., Freeman, L. A., O'Keefe, M. A., Saxton, W. O., and Wood, G. J. *Ultramicroscopy* **18**, 63-76 (1985).

3. Gronsky, R. *38th Ann. Proc. Electron Microscopy Soc. Amer., San Francisco*, 2-5 (1980).

4. Veblen, D. R., and Buseck, P. R. *Science* **206**, 1398-1400 (1979).

5. O'Keefe, M. A., Buseck, P. R., and Iijima, S. *Nature* **274**, 322-324 (1978).

6. Amos, L. A., Henderson, R., and Unwin, P. N. T. *Prog. Biophys. Molec. Biol.* **39**, 183-231 (1982).

7. Glaeser, R. M. *Ann. Rev. Phys. Chem.* **36**, 243-275 (1985).

8. Henderson, R., and Unwin, P. N. T. *Nature* **257**, 28-32 (1975).

9. Henderson, R., Baldwin, J. M., Ceska, T., Zemlin, F., Beckmann, E., and Downing, K. H. *J. Mol. Biol.* **213**, 899-929, (1990).

10. Hovmöller, S., Sjögren, A., Farrants, G., Sundberg, M., and Marinder, B.O. *Nature* **311**, 238 - 241, (1984).

11. Smith, J. V. *Amer. Mineral.* **53**, 1139-1155 (1968).

12. Kilaas, R., Proc. *45th Ann. Meeting EMSA, Baltimore*, 66 - 69, (1987).

13. Hetherington, C. J. D., Nelson, E. C., Westmacott, K. H., Gronsky, R., and Thomas, G. *Mat. Res. Soc. Symp. Proc.* **139**, 1989, p. 277-282.

Table 1 Structure factors for 10 strong reflections of staurolite

				Calculated		Experimental single reflection	
h	k	l	d(Å)	Amplitude	Phase	Amplitude	Phase
0	6	0	2.77	1.000	0°	1.000	9.1°
0	2	2	2.68	0.277	180°	0.308	169.8°
0	4	2	2.34	0.113	0°	0.186	17.4°
0	6	2	1.98	0.505	0°	0.361	-10.1°
2	0	2	2.30	0.344	180°	0.309	-177.9°
3	1	0	2.59	0.263	180°	0.627	171.7°
3	3	0	2.37	0.618	0°	1.228	-9.9°
3	5	0	2.06	0.060	180°	0.144	159.9°
2	6	0	2.26	0.400	180°	0.460	174.8°
1	3	2	2.40	0.832	0°	1.092	-11.2°

FIGURE CAPTIONS

Fig. 1. Images of the structure of staurolite viewed along [001]. JEOL ARM-1000 operating at 800 kV, Scherzer focus. *a* Experimental image in thin area (< 40Å). *b* Image reconstructed using structure factors from the computed Fourier transform of *a*. *c* Multibeam dynamic contrast calculation[12] assuming the structure of staurolite, microscope conditions as described above and specimen thickness of 30Å. **XBB911-549.**

Fig. 2. (*hk0*) diffraction patterns of staurolite. *a* Experimental selected-area diffraction pattern. *b* Corresponding calculated pattern. *c* Experimental optical diffractogram from the image in Fig. 1*a* displaying intensity to 1.4Å (arrow). Rings are due to amorphous contribution. *d* Calculated diffractogram; same conditions as for Fig. 1*c*. **XBB911-548.**

Fig. 3. Surface representation of the three-dimensional Coulomb potential in a full unit cell of staurolite, at a density level that displays all fully occupied cations and oxygens. Partially occupied sites have a density below the cutoff for this surface, giving a rather open appearance to the structure. View is close to [001]. **XBB911-547.**

Fig. 4. Sections displaying the Coulomb potential as derived from the three-dimensional structure reconstruction. *a,c* Sections at z = 0 and at z = 0.25 corresponding to a slice 0.2Å thick. *c,d* Corresponding crystal structures at z = 0 and z = 0.25, indicating cation and oxygen positions. *e* Schematic polyhedral representation with Al octahedra, and Si and Fe tetrahedra. **XBB900-10026.**

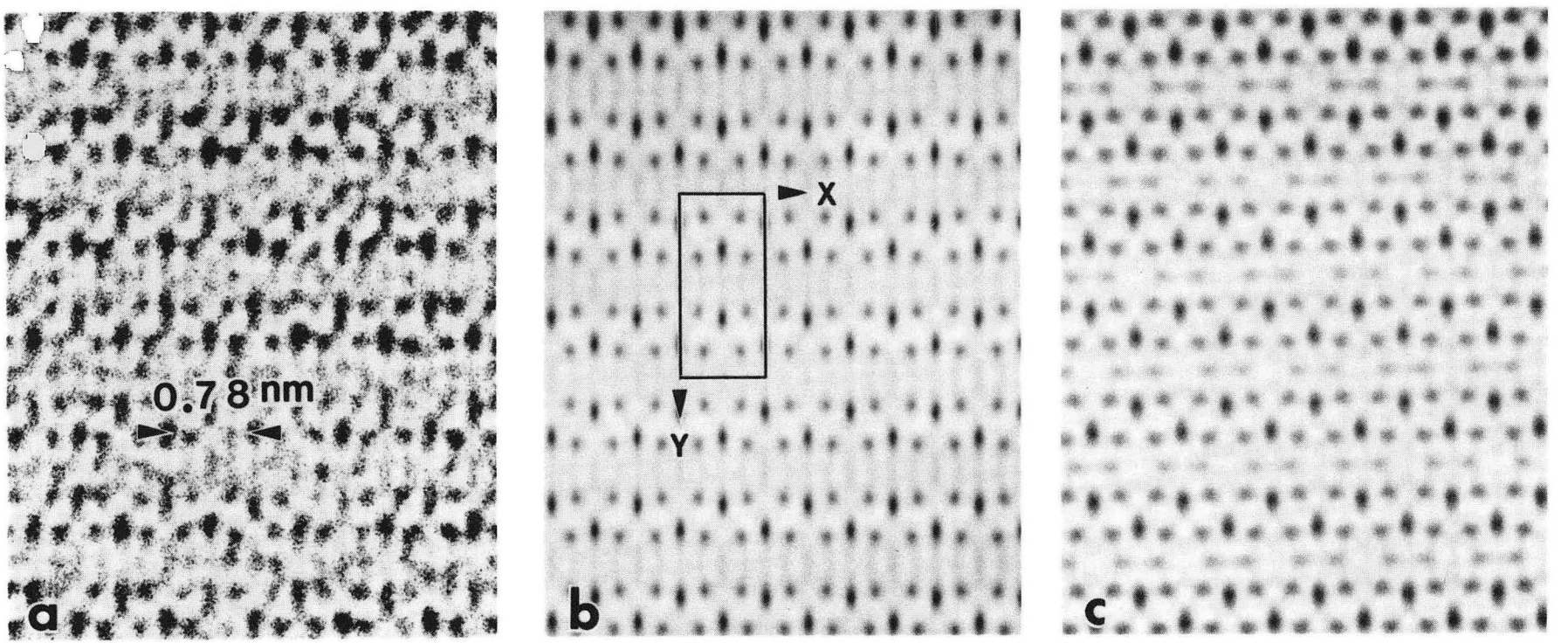

XBB 911-549

Figure 1

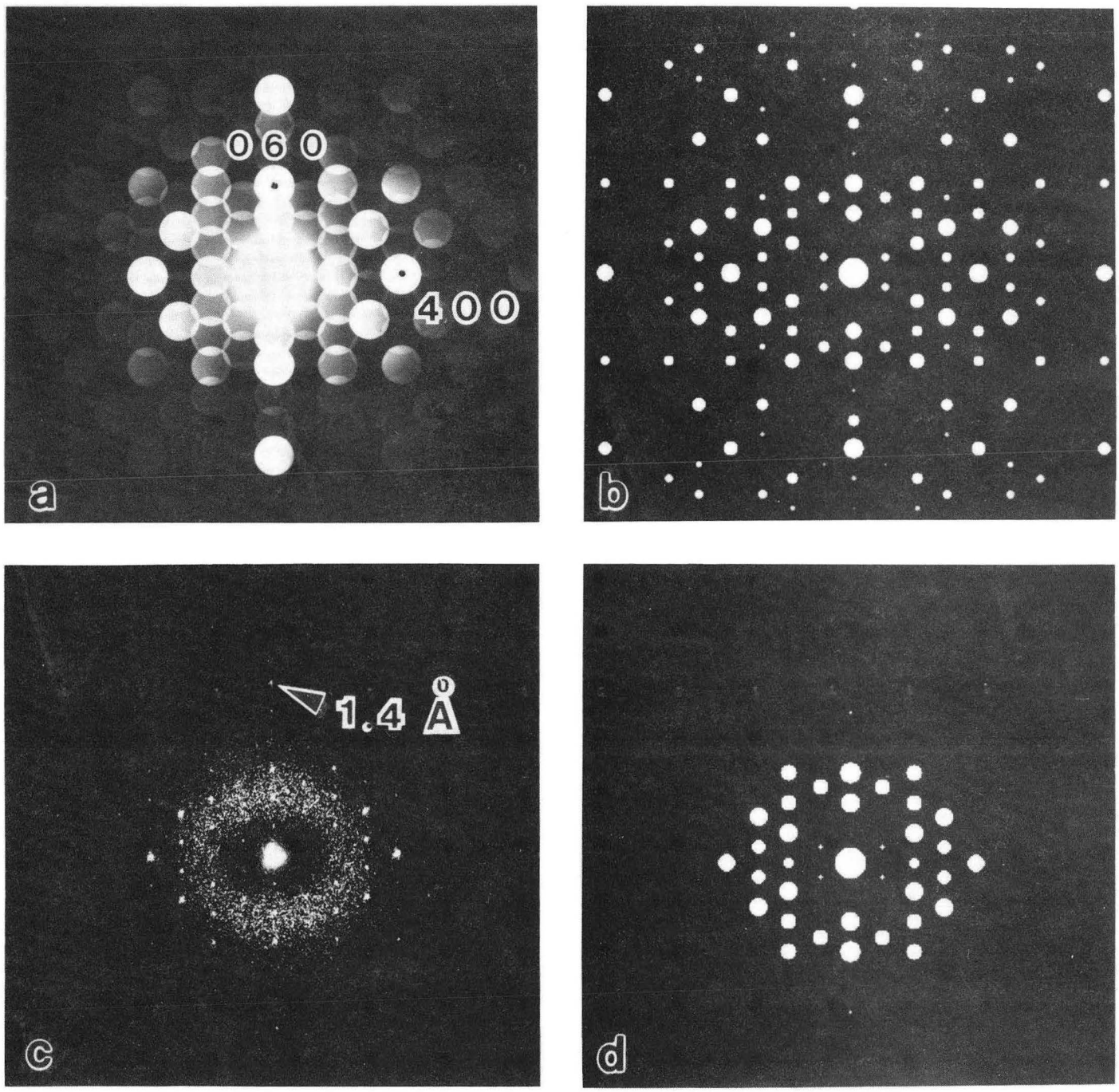

XBB 911-548

Figure 2

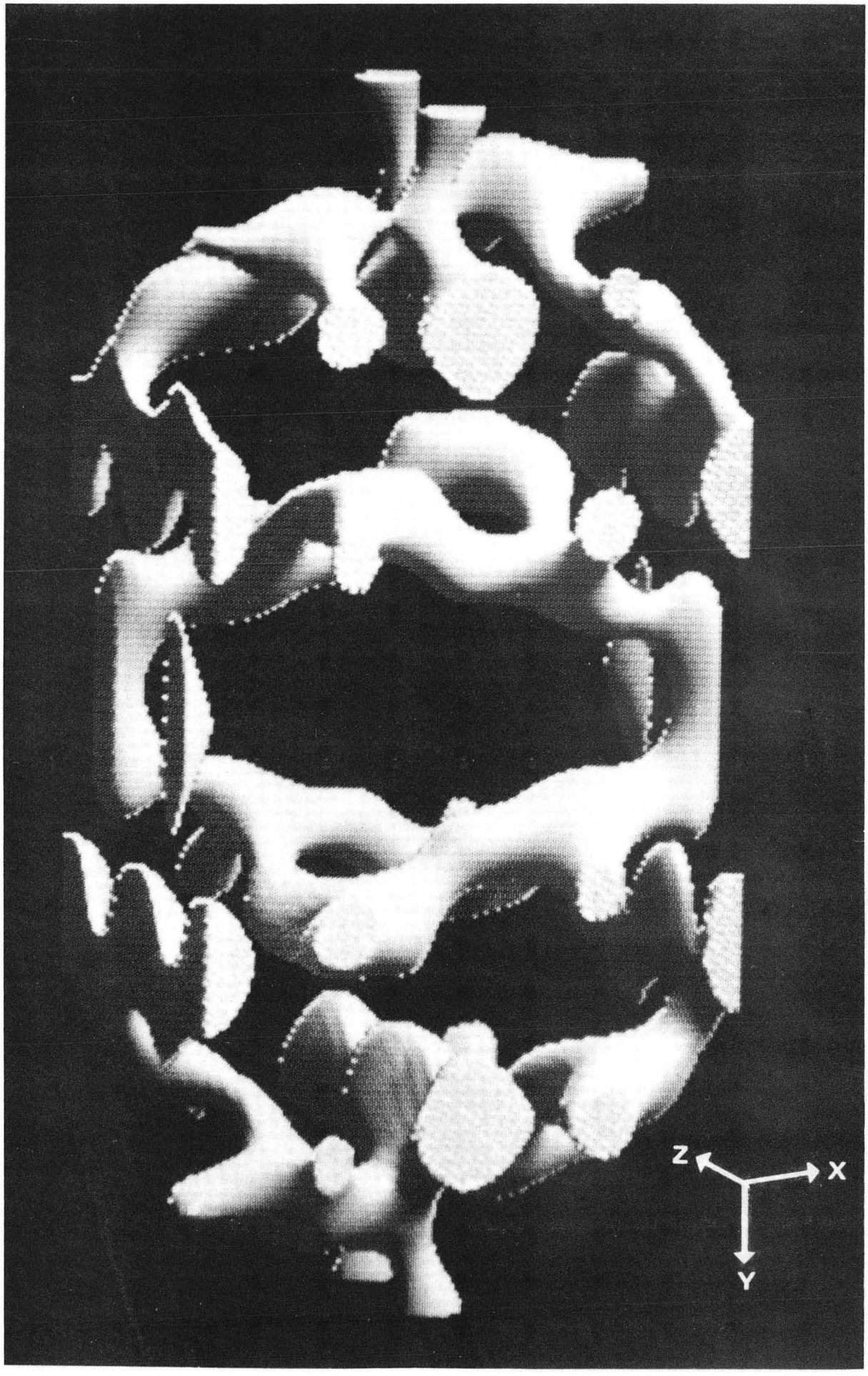

Figure 3

XBB 911-547

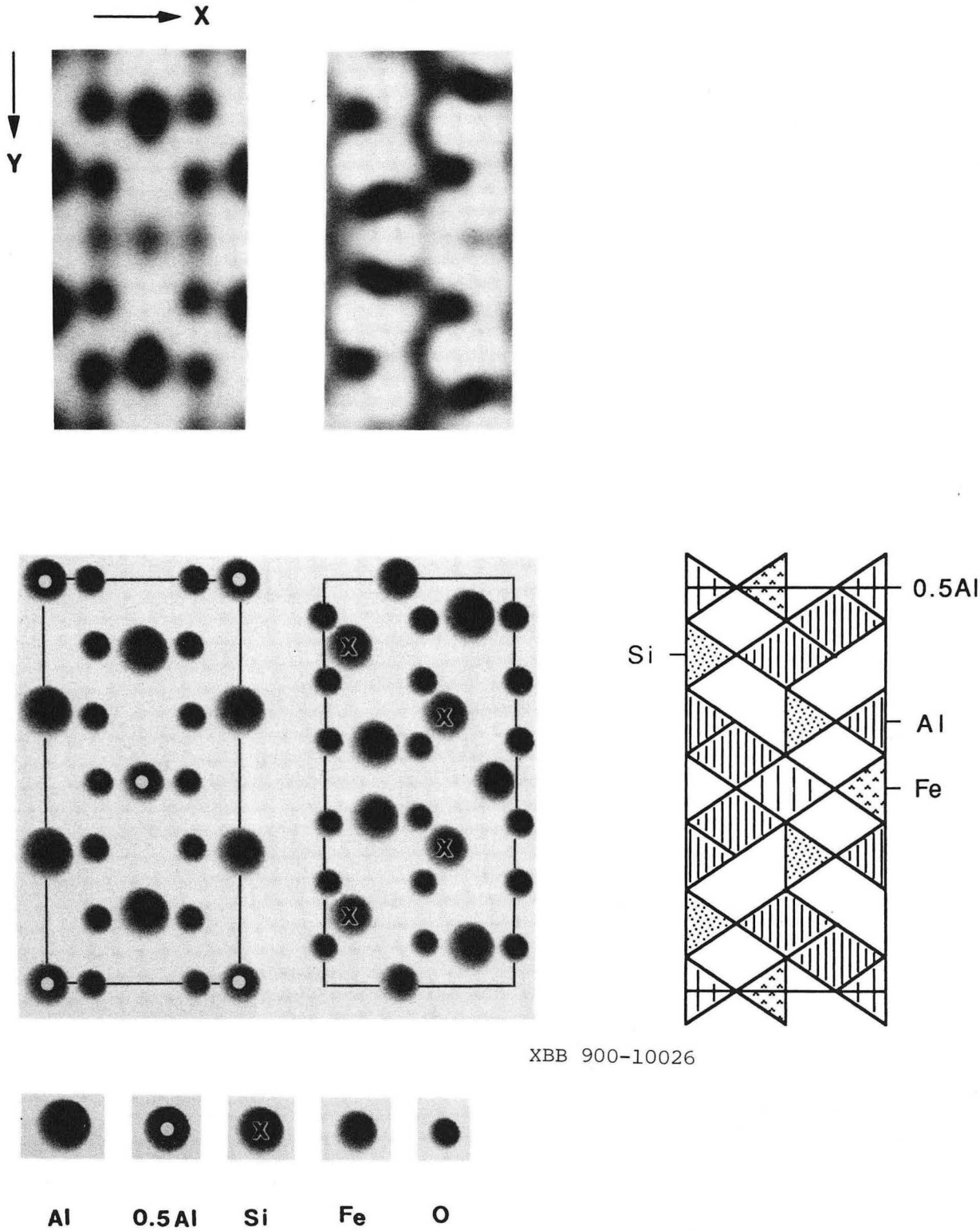

XBB 900-10026

Figure 4

LAWRENCE BERKELEY LABORATORY
UNIVERSITY OF CALIFORNIA
TECHNICAL INFORMATION DEPARTMENT
BERKELEY, CALIFORNIA 94720